



Testing magnetic tracers as indicators of sediment transport in a wave flume experiment

SORAIA ROMÃO* · † , JOÃO CASCALHO* , CAROLINE C. FERREIRA* · † · ‡, ERIC FONT* · §, RUI TABORDA*, PAULO A. SILVA†, JOÃO F. DUARTE¶ and FRANZISKA STAUDT** · † · †

*Departamento de Geologia, Faculdade de Ciências, Instituto Dom Luiz (IDL), Universidade de Lisboa, Campo Grande 1749-016, Lisboa, Portugal (E-mail: srromao@fc.ul.pt)

†Departamento de Física, Centro de Estudos do Ambiente e do Mar (CESAM), Universidade de Aveiro, Campus de Santiago 3810-193, Aveiro, Portugal

‡Observatório Oceânico da Madeira, Agência Regional para o Desenvolvimento da Investigação, Tecnologia e Inovação (ARDITI), 9020-105, Funchal, Portugal

§Departamento de Ciências da Terra da Faculdade de Ciências e Tecnologia, Instituto Dom Luiz, Universidade de Coimbra, Rua Sílvio Lima 3030-790, Coimbra, Portugal

¶Instituto Hidrográfico, Rua das Trinas, 49 1249-093, Lisboa, Portugal

**Forschungszentrum Küste, Leibniz Universität Hannover and Technische Universität Braunschweig, Merkurstraße 11 30419, Hannover, Germany

††DHI A/S, Agern Allé 5 2970, Hørsholm, Denmark

Associate Editor – Lawrence Amy

ABSTRACT

The *in situ* measurement of sediment transport in wave-dominated environments presents significant challenges and currently often relies upon the use of fluorescent sediment tracers. However, this method is constrained by challenges in conducting unbiased and representative sampling, as well as facing overall logistical complexities and labour-intensive procedures. Whilst other tracer techniques are available, such as using magnetic tracers, their performance in tracking sediment transport has not been quantified. The objective of this study is to assess the effectiveness of magnetic tracers in evaluating net transport rates and tracer dispersal patterns. Conducted in a controlled large wave flume, the experiments simultaneously employed fluorescent and magnetic tracers, allowing a comprehensive comparison of the tracers' dispersion patterns and the net transport rates. Results show that the dispersal of magnetic and fluorescent tracers displays a high degree of spatial coherence in both horizontal and vertical dimensions. Similarly, net transport rates are comparable (<16% difference), both showing net transport in the direction of the wave propagation (towards onshore) driven by non-linear and streaming effects. Magnetic tracer recovery rate (49%) was lower than for fluorescent tracers (73%) and is attributed to the loss of magnetic ink from particles; an aspect of the magnetic technique that requires improvement. This study therefore indicates that the use of magnetic tracers to quantify sediment transport is an effective method with the advantages of being significantly less labour-intensive than using the commonly applied fluorescent sediment tracer method.

Keywords Flume experiment, isothermal remanent magnetization, magnetic susceptibility, magnetic tracers, sediment tracking, sediment transport.

INTRODUCTION

Since the middle of the 20th century, sediment tracking has been used extensively to monitor or detect patterns of transport in natural environments (e.g. Pantin, 1961; Crickmore, 1976; Miller & Komar, 1979; Black *et al.*, 2007). Sediment tracer studies provide valuable insights into sediment transport dynamics, improving the knowledge of sediment circulation, enabling effective planning, and monitoring of sand nourishments, assessment of connectivity between potential sediment sources and sinks, or proper dimensioning of structures for coastal protection (Silva *et al.*, 2007; Bosnic *et al.*, 2017; Pearson *et al.*, 2021). The technique relies upon the injection of natural or artificial particle tracers into a studied area and their subsequent recovery and analysis in the laboratory or, alternatively, their *in situ* determination. In coastal environments, the use of sediment tracers has proved to be a reliable technique for the study of sediment transport, both in terms of a Eulerian approach determining net transport rates, and a Lagrangian approach tracking sediment particles (Silva *et al.*, 2007; Bosnic *et al.*, 2017; Wilson, 2018; Pearson *et al.*, 2021). Over the past three decades, various alternative methodologies for measuring sediment transport have emerged. However, as highlighted by Ciavola & Grotoli (2019), some approaches like fluorescent tracers and radio frequency identification types remain unparalleled in their versatility and applicability across a wide range of temporal and spatial scales. White (1998) estimated the accuracy of several methods based on subjective judgement, reported experiences of other studies, and on objective quantitative comparison of the different techniques in the same experiments. According to this author, sediment tracers are moderately accurate in comparison to more accurate methods, such as sediment traps or optical and acoustic techniques. Sediment tracers have significant limitations in terms of sampling their distribution, overall logistics, tracer injection, and are time-consuming and labour-intensive procedures. However, sediment tracer studies are still used due to the lack of a better alternative for monitoring sediment transport (White, 1998; Black *et al.*, 2007).

Sediment tracking experiments began during the 1950s with radioactive and fluorescent-marking techniques (Ingle, 1966). Radioactive sand provided reliable and valuable information about sand transport in natural systems (Inman

& Chamberlain, 1959; Abecasis *et al.*, 1962; Drapeau & Long, 1985; Christensen & Bhunia, 1986). However, this method is no longer recommended due to safety concerns for human health and the environment (Ingle, 1966; Black, 2012). Since the 1960s, sand coated with fluorescent paint, dye or ink has become the standard particle tracking method (Abecasis *et al.*, 1962; Yasso, 1966; Vila-Concejo *et al.*, 2004; Black *et al.*, 2007; Silva *et al.*, 2007; Bosnic *et al.*, 2017; Ciavola & Grotoli, 2019).

A number of studies use magnetic particles for tracking sediment transport (Gallaway *et al.*, 2012; Pearson *et al.*, 2021). There are three main types of magnetic materials: (i) diamagnetic (for example, quartz and calcite); (ii) paramagnetic (for example, phyllosilicates); and (iii) ferromagnetic (for example, iron oxides like magnetite, hematite and goethite) particles. Diamagnetic particles are not attracted by an external magnetic field and have negative to very low magnetic susceptibility. Paramagnetic and ferromagnetic particles are attracted to an external magnetic field and have been used previously as tracers in sediment tracking studies (see review in Black *et al.*, 2007). Ferromagnetic particles are the most suitable tracer due to their high magnetic susceptibility and their ability to remain magnetized by an external field, even when the imparted field is removed (remanent magnetization). Paramagnetic and ferromagnetic particles can be measured directly in the field using a portable magnetic susceptibility meter (for example, Bartington Instruments) or collected and separated using electromagnets. Magnetic susceptibility measurements are cost-effective and time-efficient. However, measuring their remanent magnetization or the isothermal remanent magnetization (IRM), as used in this study, requires field sampling for subsequent measurement in the laboratory. Different kinds of magnetic tracers include natural iron-rich sand (Pantin, 1961), magnetically enhanced paramagnetic sand or mudstone heated up to 500 to 900°C (Oldfield *et al.*, 1981; van der Post *et al.*, 1995), plastic beads coated with magnetic powder (Ventura *et al.*, 2001) and dual signature (fluorescent and magnetic) tracers (Black *et al.*, 2007; Pearson *et al.*, 2021).

While magnetic tracers have found applications in sediment transport studies, a systematic evaluation of their performance, particularly in comparison to the standard fluorescent technique, remains unexplored. This study aims to address this gap by assessing various application methods, including the analysis of IRM curves

and magnetic susceptibility (χ). This work investigates the use of magnetic tracers to measure sediment transport in a large flume experiment, and to compare the results with those obtained by standard fluorescent tracers. Here, sand particles coated with a commercial magnetic ink were used to test their viability as a magnetic tracer by conducting flume experiments in which sand and tracer were transported under regular, trochoidal waves. Two different magnetic techniques, SIRM (saturation of the IRM curve) and magnetic susceptibility, were used to quantify the concentration of magnetic tracers contained in the samples. The spatial distribution pattern and recovery rates of the magnetic tracers with standard fluorescent tracers were compared.

METHODS

The experiment was carried out in the Large Wave Flume (Großer Wellenkanal – GWK) of the FZK – Forschungszentrum Küste (Leibniz Universität Hannover and Technische Universität Braunschweig, Germany) between 11 and 15 June 2018. The flume has dimensions of 330 m (length) \times 5 m (width) \times 7 m (depth). The test section was located in the middle of the channel from $X=96.60$ m to $X=126.96$ m (where datum $X=0$ m corresponds to the position of the wave paddle) with dimensions 30.36 m length, 5.00 m

width and 0.90 m height (from the flume bottom; Fig. 1). The bottom of the flume in the test section was covered with a 0.60 m base layer (sand covered by geotextile) and a 0.30 m thick test sand bed. The bed was smoothed and levelled at about 0.92 m (between 0.90 m and 0.95 m) height from the flume bottom. For this study, an array of three Acoustic Doppler Velocimeters (Nortek Vector ADV, Nortek, Norway) in the middle of the test section was used to record hydrodynamic data, while bed profiles were collected with echo sounders in between wave runs (see van der Werf *et al.*, 2019, and Ferreira, 2022, for setup details and further instrumentation, that is not the subject of this study).

The sand used in the experiments was provided by the company Schlingmeier Quarzsand (Schwülper, Germany) and comprised a mixture of 75% coarse sand and 25% fine sand, with median values (D_{50}) of 0.58 mm and 0.21 mm, respectively (Fig. 2A). The sand was dominantly composed of quartz with the chemical analysis provided by the manufacturer indicating a composition of 99.6% SiO_2 and a density of 2650 kg m^{-3} . Grain-size data provided by the manufacturer, applying the statistical logarithmic method of moments (Folk, 1966; Blott & Pye, 2001), indicate that the coarse sand population is very well-sorted (0.26ϕ) and positively skewed (0.64ϕ), and the finer population is well-sorted (0.41ϕ) and positively skewed (0.59ϕ).

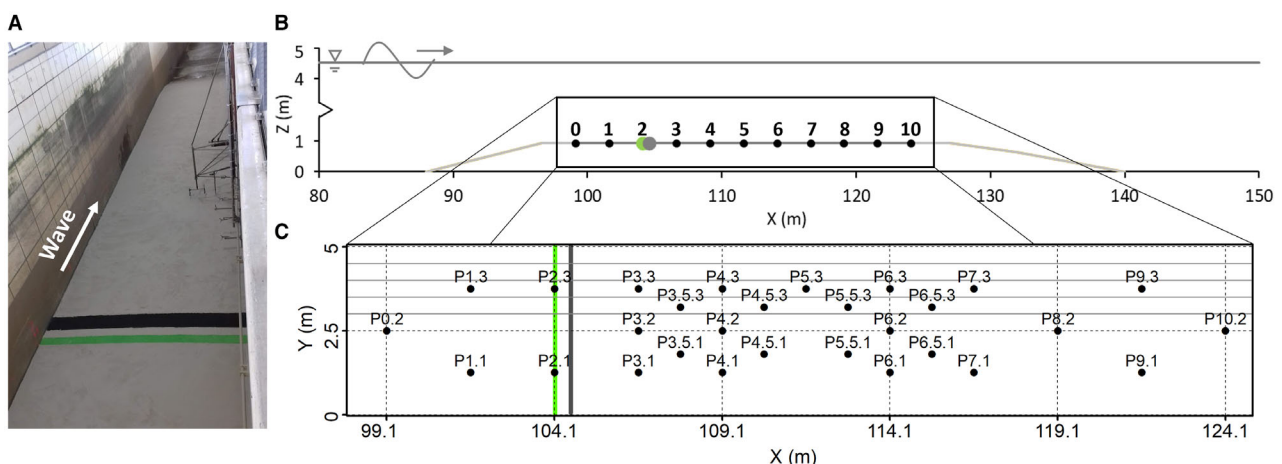


Fig. 1. (A) Photograph of the Large Wave Flume of the FZK – Forschungszentrum Küste, Leibniz Universität Hannover. The black and green strips correspond to the magnetic and fluorescent tracers at the injection lines, respectively. (B) Vertical cross-section of the flume with the area of the test section covered by the test sands and the position of the source injection of the magnetic (grey circle) and fluorescent (green circle) tracers. (C) Enlargement of the area of the test section showing the position of the samples. The solid horizontal lines represent the location of the bed profiles spaced 0.5 m apart across the flume.

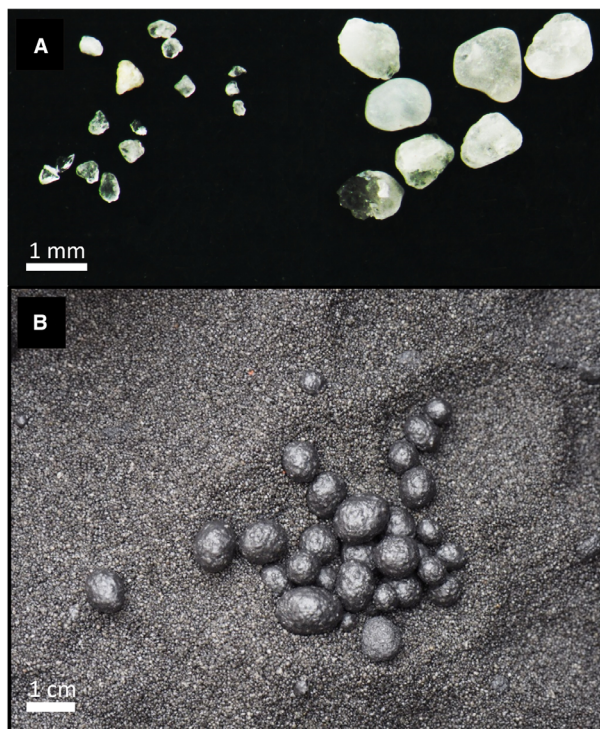


Fig. 2. (A) Photograph of the sand used in the flume experiment: on the left the presence of coarse sand particles ($D_{50} = 0.58$ mm) and on the right the presence of the fine sand particles ($D_{50} = 0.21$ mm). Most of the particles correspond to milky and hyaline quartz mineral. (B) Photograph of the magnetic tracer particles showing larger agglomerated pellets that formed during the coating process, noting that these were removed by sieving before the flume experiment.

Preparation of tracers

The magnetic tracer (MT) was composed of the coarser sand fraction ($D_{50} = 0.58$ mm). The uncoated sand was placed in a concrete mixer with 3.75 l of magnetic ink. The ink is a water-based INFANTIL IMAN magnetic ink from ALP (Barcelona, Spain; <https://pinturas-alp.com/>), which contains magnetic non-oxidizable pigments with a density of 2.1 ± 0.05 kg l⁻¹. To find the optimum ink/sediment ratio, several experiments were previously made in a laboratory setting using a small sand volume. It was found that the optimum ink dosage is *ca* 10% of the sediment volume, which results in a suitable coating of the particles and, simultaneously, avoids particle aggregation. The use of the concrete mixer in continuous rotation (about 8 h) allows a uniform coating of the grains, while

drying them at the same time. The aggregates (mostly corresponding to aggregation pellets) formed during the coating processes were removed using a 2 mm sieve (upper limit of the sand grain size class; Fig. 2B). To test whether the ink significantly affects the density of sand particles, a laboratory test of density was carried out using sodium polytungstate with a density of 2900 kg m⁻³; a dense liquid normally used for the separation of heavy and light minerals (Garzanti & Andò, 2019). Results show that the weight percentage of heavier particles (i.e. those with a density >2900 kg m⁻³) varies from 0.21% for the test sand to 2.43% for the sand coated with magnetic ink.

The fluorescent tracer was composed of heterometric fluorescent sand comprising 75% coarse sand and 25% fine sand. This sand mixture was coated with a fluorescent green ink (from Atomlac Industries, Villenave-d'Ornon, France) using a concrete mixer with a combination of ink and cellulose diluent, in the proportion of 40% mass of ink to 60% of diluent following Silva *et al.* (2007).

Flume experiment

Sixty kilograms of magnetic tracer were placed over a strip of 5.0 m (width) × 0.5 m (length) and 0.02 m thickness, at a distance of 104.6 m from the wave paddle (Fig. 1A and B). The flume was filled with fresh water up to 4.4 m, resulting in a water column of 3.5 m above the test section. In addition, 25 kg of fluorescent tracer was placed in the test section at $X = 104.1$ m (Fig. 1A and B).

The hydrodynamic conditions were chosen following the previous work of Schretlen (2012) in the GWK flume involving regular trochoidal waves with 1.5 m height and a period of 7 s. Figure 3 presents the average wave velocity profile measured by an ADV. These waves generate near-bed orbital velocities with significant velocity skewness, $R = 0.63$ (high onshore peak velocity, lower offshore peak velocity) and acceleration skewness, $B = 0.53$ (Ferreira *et al.*, 2023) that acts as a driving mechanism for onshore (in the direction of wave propagation) sediment transport. Five runs of waves were performed, each run propagates 200 waves and has a duration of 1400 s (23.3 min).

Between each run (i.e. at still water level), bed profiles were measured with echo sounders installed on a mobile platform that moved over the test section. A total of four profiles was

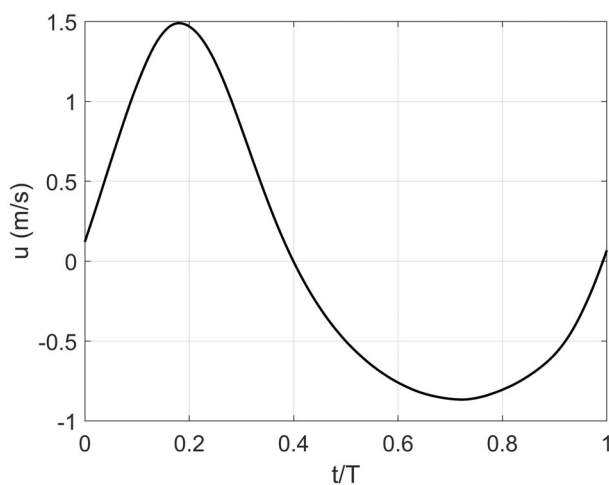


Fig. 3. Time series of the ensemble average wave velocity for the experiment measured by the Acoustic Doppler Velocimeter (ADV), at 1.28 m above the bed.

obtained at locations across the flume: $Y = 3.0$ m, 3.5 m, 4.0 m and 4.5 m (Fig. 1C).

After the five wave runs and draining of the flume, a detailed sampling of the bed material was carried out. Twenty-nine cores were collected using PVC tubes of 0.50 m length and 0.05 m diameter, arranged as shown in the sampling grid in Fig. 1C. The cores were then sliced into five layers (D1 to D5) with the uppermost surface layer, D1, being 1 cm thick, and the underlying layers being 2 cm thick. This procedure resulted in a total of 145 samples. These sediment samples were used to estimate the concentrations of both magnetic and fluorescent particles throughout the sediment column at each point.

Magnetic measurements

Samples were prepared at the laboratory of the Geology Department of the Portuguese Hydrographic Institute (Lisboa, Portugal). They were washed with distilled water on a 63 μm sieve to remove silt-sized and clay-sized particles and dried in an oven (at 40°C). Magnetic measurements were then performed at the Paleomagnetism Laboratory of the Department of Earth Sciences of the University of Coimbra (Coimbra, Portugal), consisting of measurements of magnetic susceptibility and the acquisition of IRM curves. Samples were placed in standard (8 cm³) cubic plastic boxes. Magnetic susceptibility (χ) is the quantitative measure of the extent to

which a material may be magnetized in relation to a given applied magnetic field, and provides information on the contribution, in relative abundance, of diamagnetic (for example, quartz), paramagnetic (for example, clays) and ferromagnetic minerals (for example, iron oxide such as magnetite). Since magnetic susceptibility of ferromagnetic particles, like the magnetic tracers used here, is several orders of magnitude higher than the magnetic susceptibility of diamagnetic materials (i.e. quartz sand), the values of magnetic susceptibility of the samples collected after the flume experiment are linearly proportional to the concentration of magnetic tracers. Magnetic susceptibility was measured with a MS2B Bartington apparatus (Bartington Instruments, Witney, UK) and the results are reported relative to volume (K in SI) or mass (χ in m³ kg⁻¹).

Isothermal remanent magnetization (IRM) is a magnetization resulting from the application of an applied direct current field, and provides information about ferromagnetic particles only, i.e. the magnetic tracers. IRM curves were acquired after imparting stepwise-increasing uniaxial fields (typically *ca* 30 steps) with an impulse magnetizer (model IM-30; ASC Scientific, Narragansett, RI, USA) and the remanence was measured using a Molspin magnetometer. The maximum applied field was 1.2 T. IRM curves were treated by a cumulative log-Gaussian function (Kruiver *et al.*, 2001) or a skewed generalized (log) Gaussian function with the Max UnMix program (Maxbauer *et al.*, 2016) to isolate the contributions of the different populations of magnetic grains. This analysis provides information about: (i) the value of the saturation isothermal remanent magnetization (SIRM); (ii) the coercivity (noted here as $B_{1/2}$ in mT), which corresponds to the value of the field imparted to reach half of the saturation; and (iii) the dispersion parameter (DP), which provides information about the relative distribution of the magnetic size. At first approximation, SIRM is proportional to the relative abundance of ferromagnetic particles, whereas $B_{1/2}$ and DP mainly depend on nature and grain size, respectively. IRM curves were acquired for non-coated sand and for five pilot samples containing magnetic tracers in order to obtain the value of the field at which the magnetization reaches saturation. This field was then imparted to obtain the values of the SIRM of the rest of the samples.

Tracer calibration curves

The conversion of the measured values of SIRM and χ into tracer mass concentration was

achieved using a calibration curve. The curve was constructed by measuring SIRM and χ values of samples with a known concentration (ratio between mass of tracer and mass of sand) of magnetic tracers. To fulfil this objective, a set of 22 samples was prepared with concentrations from 0 to 2%, with successive increment steps of 0.1%, for a total mass of 20 g. The mass was measured with a precision balance with an accuracy of $\pm 0.1 \times 10^{-3}$ g. The derived empirical equations of the calibration curves allow the conversion of the values of SIRM and χ into concentration (Fig. 4).

Fluorescent tracer detection

The detection of the fluorescent tracer was done at the laboratory of the Physics Department of the University of Aveiro (Aveiro, Portugal). Samples

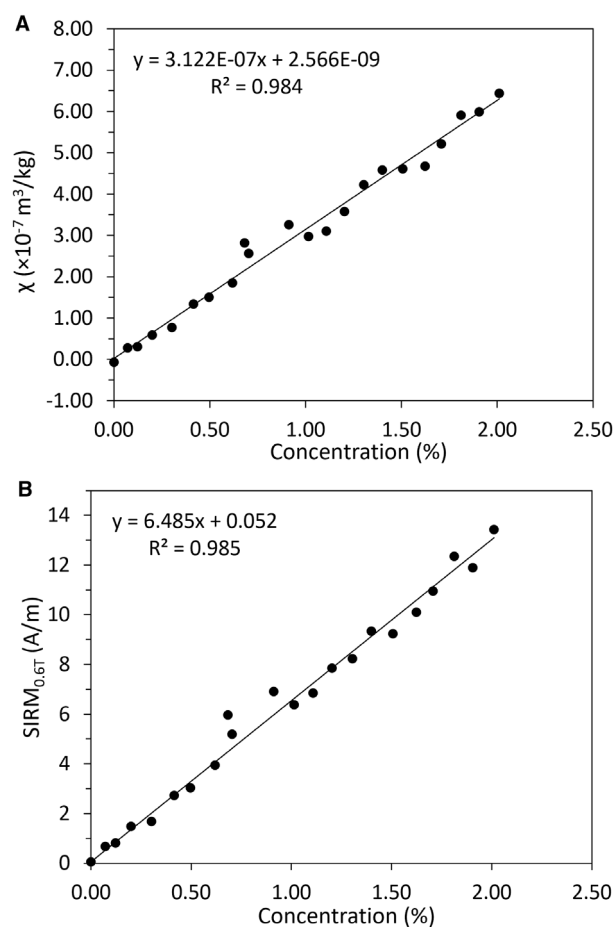


Fig. 4. Calibration curves for the magnetic tracer concentration with (A) mass-specific magnetic susceptibility (χ) and (B) isothermal remanent magnetization at saturation (SIRM_{0.6T}).

were placed in a black tray and digitally photographed under visible and UV light with a fixed digital camera, where each photograph covers an area of 6.0×10^{-3} m². The detection of fluorescent tracer particles and their counting in each photograph was performed automatically with a MATLAB toolbox through an image processing routine referred to by Bosnic *et al.* (2017), available at <http://sandcode.rd.ciencias.ulisboa.pt/ImageAnalysis.html>. Because the samples were initially well-mixed, the results are representative of the tracer's concentration existing in the whole sample. The image analysis procedure obtained the tracer concentration in dimensionless values calibrated using a regression line that results from the correlation between the tracer mass concentration (ratio between the successive increasing masses of tracer particles and the fixed mass of native sediment), and the area concentration (ratio between the total number of pixels of tracer particles and the fixed number of pixels of each photograph). For comparison with magnetic sand tracers, only the fluorescent coarse sand fraction was used (corresponding to a mass of 18.75 kg), because the finer fraction exhibited a different behaviour (see Ferreira *et al.*, 2023, for details).

Sediment transport and tracer recovery rates

The spatial distribution of the depth-averaged tracer concentration (C) was obtained by interpolation using the inverse distance squared weighted method. The along-channel displacement of tracer centre of mass (x_{cm}) at the end of the experiment was obtained according to the equation:

$$x_{cm} = \frac{\sum_i^n C(x) \times x}{\sum_i^n C(x)} \quad (1)$$

where x is the along-channel coordinate ($x=0$ corresponds to the injection line) and n is the number of bed samples. The centre of mass average velocity is calculated by dividing the centre of mass displacement by the duration of the experiment, a total of 7000 s (five runs of 1400 s each). The net transport rate was estimated by the product of the centre of mass velocity and the thickness of the sampled layer, $h=0.09$ m [see Ferreira, 2022, for details].

The tracer recovery was estimated based on the spatial interpolation of tracer concentration over the test section (covering an area of 30 m length and 5 m width). The interpolation was

based on the Thiessen polygon method (Mu, 2009). The tracer mass in each polygon (m_p) was computed as:

$$m_p = a \times h \times C \times \rho_s \times (1-p) \quad (2)$$

where a is the area of each polygon, C is the depth-averaged concentration, h is the thickness of the sampled layer, ρ_s is the sand density ($\rho_s = 2650 \text{ kg m}^{-3}$) and p is the sand bed porosity ($p = 0.4$). The tracer recovery was estimated separately for the χ , the IRM and fluorescent data. The computation of the tracer recovery rate was based on the following expression:

$$R = \frac{\sum_{i=1}^j m_p}{m_t} \quad (3)$$

where m_t is the total tracer mass (60 kg) and j is the number of polygons. The vertical concentration was assessed for the surficial layer D1 (0 to 1 cm depth below the bed surface) and for each of the four layers underneath D2 to D5 (1 to 3 cm, 3 to 5 cm, 5 to 7 cm and 7 to 9 cm depths below the bed surface). As all samples were referred to an uneven bottom surface (see *Bed morphology* section), the absolute sample height was estimated using the topographic profiles surveyed after the run. The sediment transport mode was estimated using the wave mobility number:

$$\psi = \frac{u_{\max}^2}{(s-1)gd_{50}} \quad (4)$$

where u_{\max} is the maximum positive velocity, s is the specific sediment density, g is the acceleration due to gravity and d_{50} is the median grain size.

RESULTS

The results described here focus on the description of the magnetic tracer results and comparison with the fluorescent tracer. A detailed description of hydrodynamics, sediment transport and morphological conditions for these laboratory experiments is presented in Ferreira (2022) and Ferreira *et al.* (2023).

Bed morphology

During the experiment, waves induced changes in bottom morphology from the initial smooth bed. Figure 5 shows the bed morphology for the initial bed, after the first run (R1) and after the

final run (R5). It may be seen that bedforms had already formed after the first run with bedforms clearly visible along all four profiles ($Y = 3.0 \text{ m}$, $Y = 3.5 \text{ m}$, $Y = 4.0 \text{ m}$ and $Y = 4.5 \text{ m}$). Results presented in Boscia (2021) for the same experiment suggest that the bedforms reached equilibrium 15 min after the beginning of the experiment. These bedforms were present along the entire test section and had a three-dimensional structure (Fig. 5), with an average height of $0.07 \pm 0.04 \text{ m}$, an average length of $0.83 \pm 0.32 \text{ m}$ and a maximum height of *ca* 0.20 m (Ferreira, 2022).

Magnetic data

The mass-specific magnetic susceptibility of uncoated sand has negative measured values of *ca* $-6 \times 10^{-9} \text{ m}^3 \text{ kg}^{-1}$, typical of diamagnetic particles (Dearing, 1999). Samples used for the calibration curves and containing between 0.07% and 2.0% of magnetic tracer have positive mass-specific magnetic susceptibility, varying from 2.73×10^{-8} to $6.44 \times 10^{-7} \text{ m}^3 \text{ kg}^{-1}$, which is typical of paramagnetic to ferromagnetic particles. This demonstrates that the presence of magnetic tracers, even in low concentrations (0.07%), increases the magnetic signal by two to three orders of magnitude. Consequently, the calibration curve (Fig. 4) shows a strong correlation ($R^2 = 0.984$) between the concentration of the magnetic tracers and mass-specific magnetic susceptibility, supporting the notion that χ can be used as a reliable indicator of magnetic tracer concentration in the present experiment. Bed samples collected in the flume after the experiment exhibited values of χ in the range of 1.43×10^{-8} to $20.06 \times 10^{-8} \text{ m}^3 \text{ kg}^{-1}$.

The SIRM values of samples containing magnetic tracers are one to two orders higher than those without magnetic tracers (Fig. 6A). The exception is sample P1.1-D4, which has SIRM values comparable to the sand without magnetic tracers (Fig. 1C; Table 1). After unmixing the IRM curves with the Max UnMix software (Maxbauer *et al.*, 2016), the sand without magnetic tracers shows a bimodal distribution (Fig. 6B), whereas the sand with magnetic tracers has a single magnetic component (Fig. 6C). Component 1 of the sand without magnetic tracer has a mean coercivity ($\log B_{1/2}$) of *ca* 1.72 mT, with DP values of *ca* 0.36 mT, typical of magnetite (Egli, 2004), while Component 2 has a $\log B_{1/2}$ of *ca* 2.7 mT (DP *ca* 0.35 mT), typical of hematite. Component 2 only contributes to less than 5% of the total remanence. Component 1 of the sand containing

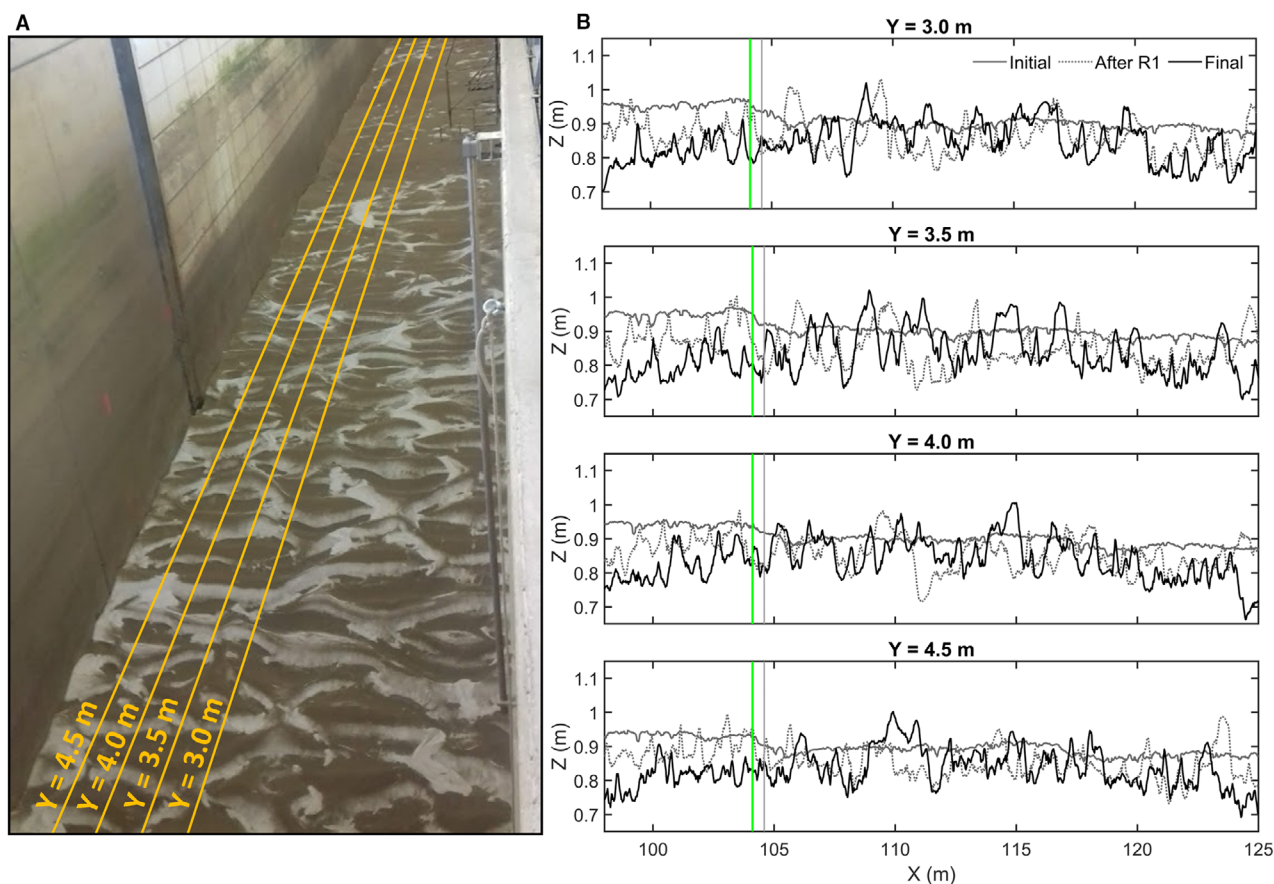


Fig. 5. (A) Photograph of the bed at the end of the experiment after draining the flume. Dark areas correspond to thin clay deposits that cover the bedform troughs (related to the deposition of fine-grained particles from river water used to fill the flume) and lighter areas correspond to the bedform crests. The yellow lines represent the location of bed profiles. (B) Bed profiles where continuous grey lines represent the initial morphology, dashed grey lines correspond to the morphology after the first run (R1) and continuous black lines represent the morphology at the end of the experiment. The green and grey vertical bars represent the injection location of the fluorescent and magnetic tracers, respectively.

magnetic tracers has a mean coercivity of 1.62 mT, with DP values of 0.31 to 0.33 mT, typical of magnetite (Egli, 2004; Fig. 6D; Table 1).

The similarity of the mean coercivity and DP values observed within the pilot samples indicates that the nature of the magnetic particles (i.e. magnetite) and the grain size do not vary significantly, and that the values of the SIRM are therefore essentially controlled by the concentration of the magnetic particles in the sample. At $B = 0.6$ T, more than 99% of the induced magnetization reaches saturation. A field of 0.6 T was applied to quantify the SIRM of all samples analysed in the flume experiment and in the calibration curve. With regard to the mass-specific magnetic susceptibility, the calibration curve shows a strong correlation

between the concentration of the magnetic tracers contained in the sample and the $\text{SIRM}_{0.6\text{T}}$ ($R^2 = 0.985$) (Fig. 4), validating the use of both χ and SIRM values as a reliable indicator of the concentration of magnetic tracers.

Tracer distribution pattern

The patterns of depth-integrated concentration of the magnetic tracer, which were estimated based on $\text{SIRM}_{0.6\text{T}}$ and χ are plotted in Fig. 7. The concentration of magnetic tracers (based on $\text{SIRM}_{0.6\text{T}}$) is higher in the middle of the test section, at a distance of 108 to 115 m from the wave paddle (Fig. 7A). The concentration decreases shoreward (to the right) and is negligible at the end of the test section (ca 124 m from the wave

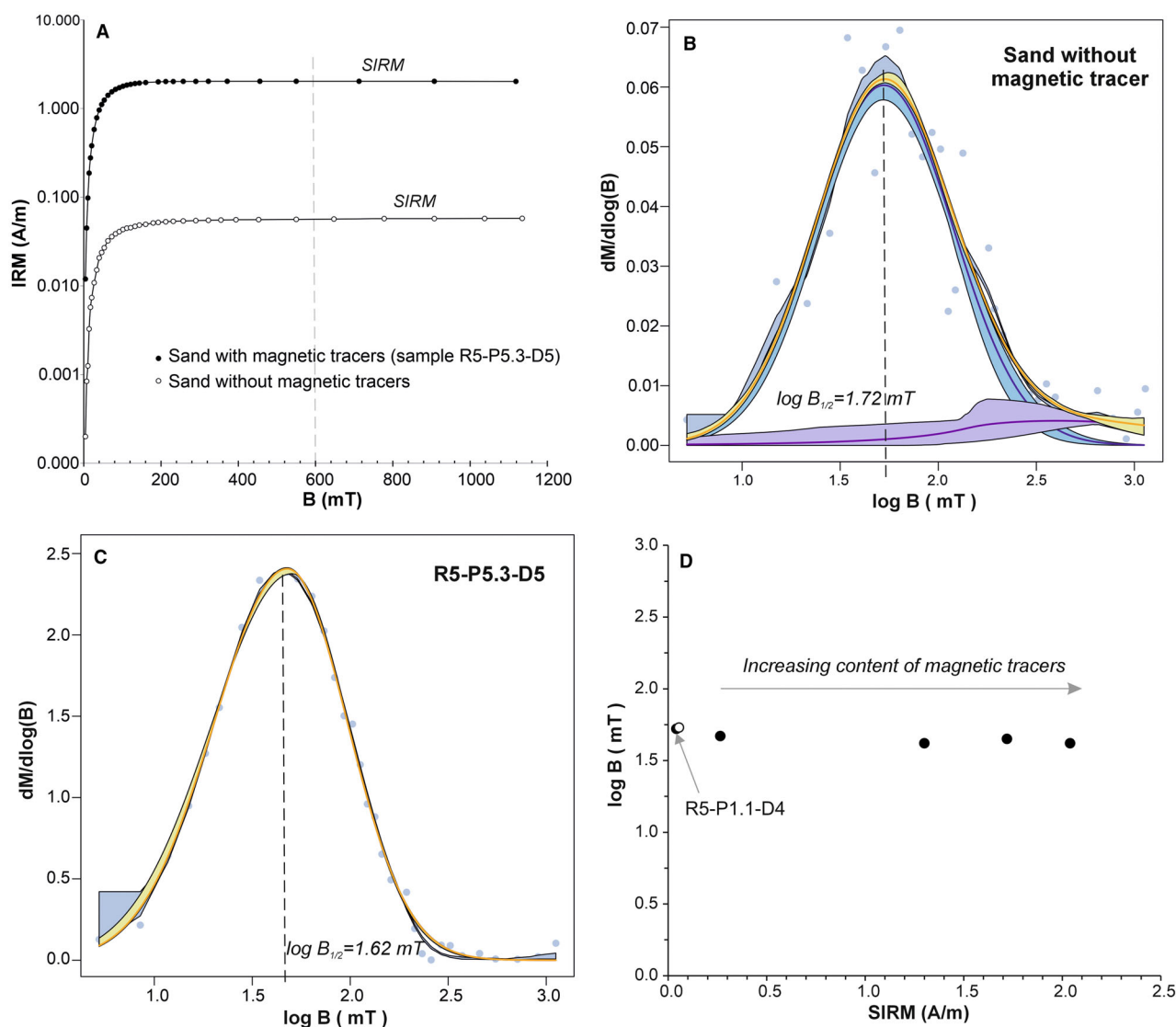


Fig. 6. (A) Isothermal Remanent Magnetization (IRM) curves for sands with and without the magnetic tracer (sample R5-P5.3-D5). SIRM is the value of the IRM at saturation. IRM curves of (B) the sand without magnetic tracer and (C) with magnetic tracer (sample R5-P5.3-D5) treated with the MaxUnmix software. $\log B_{1/2}$ (mT) corresponds to the mean coercivity of the population of magnetic grains. (D) SIRM versus $\log B_{1/2}$ of the five pilot samples (black circle) and the sand without magnetic tracer saturation isothermal remanent magnetization (open circle) showing that the SIRM increases accordingly to the content of magnetic particles.

paddle). Concentrations are very low offshore (to the left) of the injection line. The distribution of concentrations based on χ is very similar to the $SIRM_{0.6T}$ (Fig. 7B), with patterns alternating between relatively high and relatively low concentrations.

The vertical distribution of the concentration of the magnetic tracer based on $SIRM_{0.6T}$ for the samples located at $Y = 3.20$ and $Y = 3.75$ m is shown in Fig. 8A and B; these samples being

closest to the longitudinal bed profiles (Fig. 1). Given the three-dimensional nature of the bedforms, the crest and troughs of the bedforms are not uniformly distributed in the Y direction. The average value of the bed levels measured at contiguous profiles was used to estimate the height of the top of the cores. In general, the results show that concentrations are higher in the surface layers and that the cores collected near the bedforms crests show a higher

Table 1. Values of saturation isothermal remanent magnetization (SIRM), coercivity ($\log B_{1/2}$) and dispersion parameter (DP) of sand without tracer and the pilot samples containing magnetic tracers collected in the flume after the experiment. In the samples reference name, 'D' refers to the sampled layer.

Samples	SIRM (A/m)	Log $B_{1/2}$ (mT)	DP (mT)
Sand without magnetic tracer	5.55E-02	1.73	0.36
P5.3-D5	2.04E+00	1.62	0.33
P1.1-D4	4.25E-02	1.72	0.33
P3.2-D1	2.65E-01	1.67	0.31
P6.3-D3	1.72E+00	1.65	0.33
P6.3-D5	1.30E+00	1.62	0.32

variability of concentration of magnetic tracers than the cores near the troughs. Despite variations in absolute concentration values, the comparison of concentration distribution patterns along the vertical for both the magnetic and fluorescent tracers suggests a strong agreement (Fig. 8C and D). These results also show that the thickness of the active layer (the uppermost bed layer susceptible to be remobilized by waves and currents) is not uniform along the channel and reaches a thickness of at least 20 cm corresponding to the height of the largest mobile bedforms. This indicates that the sampling depth used was insufficient to encompass the entire active layer.

Sediment transport and tracer recovery rates

The passage of waves generates an oscillatory motion, resulting in back and forth movement of sediments. When the waves are asymmetrical, with higher orbital velocities under the crests and lower velocities under the troughs, a net sediment transport is induced in the direction of wave propagation (e.g. Soulsby & Damgaard, 2005). In this experiment, wave asymmetry ($R=0.63$) played a crucial role in driving the observed net sediment transport. However, it is important to note that the total particle displacement far exceeds the net displacement observed. To understand the transport regime, the mobility number may be used and was determined for the present experiment to have a value of $\Psi=231$. According to the classification

of O'Donoghue *et al.* (2006), this implies sediment transport in the transitional regime between the sheet-flow and ripple regimes (Ferreira *et al.*, 2023). However, the presence of bedforms (see *Bed morphology* section) indicates that sediment transport occurred mainly in the ripple regime (van der Werf *et al.*, 2019).

The displacement of the centre of mass, the average concentration, the tracer recovery rate for each layer and the transport rates quantified using the magnetic tracer are provided in Table 2. The data based on using the fluorescent tracer are also shown to provide a comparison of the two techniques (data also reported in Ferreira, 2022). The horizontal displacement of the centre of mass displays a uniform vertical distribution, with values roughly similar for the different approaches: 7.37 m for the $SIRM_{0.6T}$ and 7.52 m for the χ . The recovery pattern is vertically uniform [noting that the surficial layer (D1) is half as thick as the other layers (D2 to D5)]. The depth-averaged net transport rate was estimated to be $9.47 \times 10^{-5} \text{ m}^2 \text{ s}^{-1}$ based on $SIRM_{0.6T}$ measurements and $9.67 \times 10^{-5} \text{ m}^2 \text{ s}^{-1}$ based on χ measurements, both corresponding to a tracer centre of mass displacement of 6.6 cm min^{-1} in the direction of wave propagation.

DISCUSSION

Effectiveness of magnetic tracer particle recognition

The use of magnetic susceptibility (χ) and isothermal remanent magnetization ($SIRM_{0.6T}$) analysis led to consistent and comparable results for the detection of the magnetic tracers in the flume experiment. Although the composition of the magnetic particles contained in the magnetic ink is not provided by the manufacturer, the values of the mean coercivity ($B_{1/2}$) calculated based on the unmixing of the IRM curve of the sand coated with the magnetic ink are typical of magnetite (*ca* 20 to 40 mT; Egli, 2004), the most common magnetic iron oxides found in natural environments. The sand used in the experiment is essentially composed of 99% diamagnetic quartz particles (SiO_2) (i.e. negative and very low magnetic susceptibility). Thus, positive values of magnetic susceptibility of the samples, together with a strong correlation between χ and SIRM, demonstrate that the presence of the ferromagnetic magnetite pigment is the determining factor that controls the magnetic response of the tracer particles. These contrasting magnetic properties

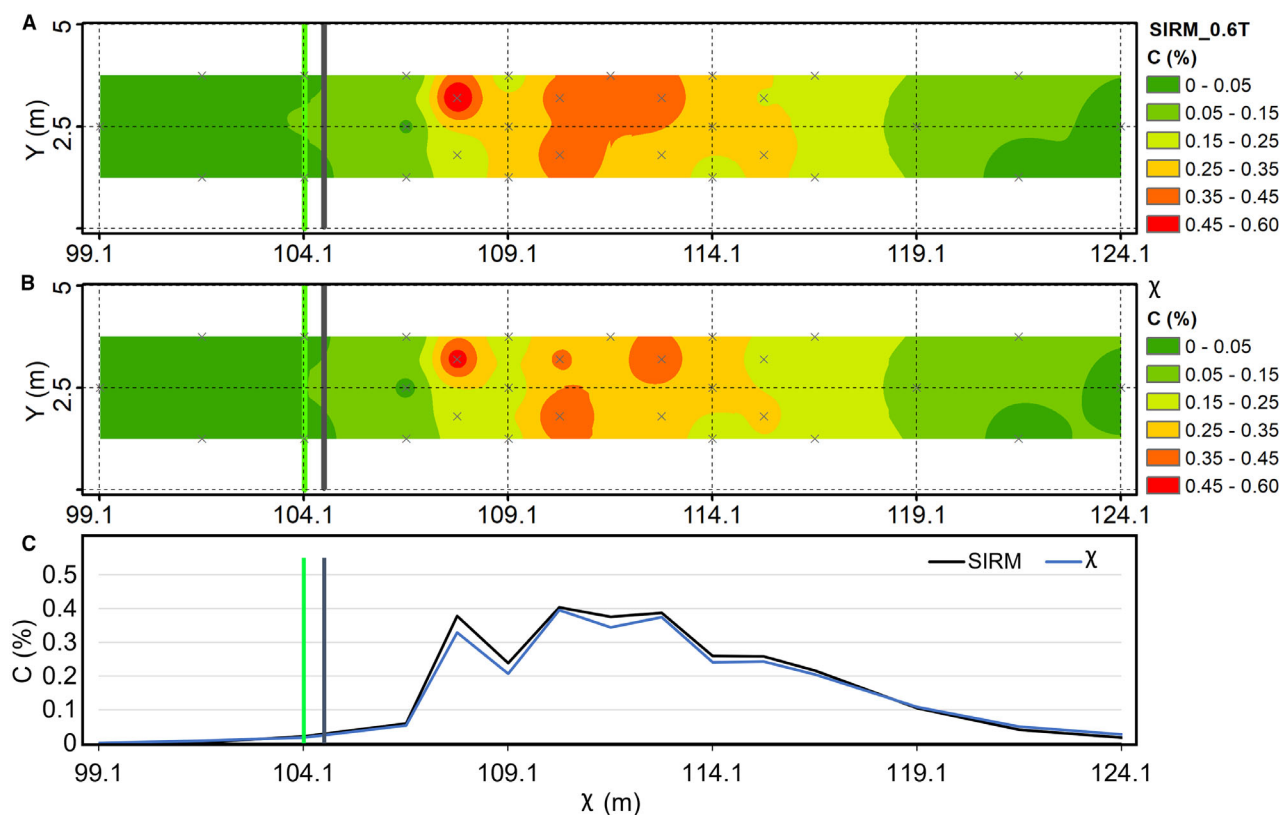


Fig. 7. Distribution of tracer concentration along the test section: (A) magnetic tracer measured by isothermal remanent magnetization (SIRM_{0.6T}); (B) magnetic tracer measured by magnetic susceptibility (χ); and (C) average streamwise concentration using both SIRM_{0.6T} and χ . The green and black lines correspond to the injection lines of fluorescent and magnetic tracers, respectively.

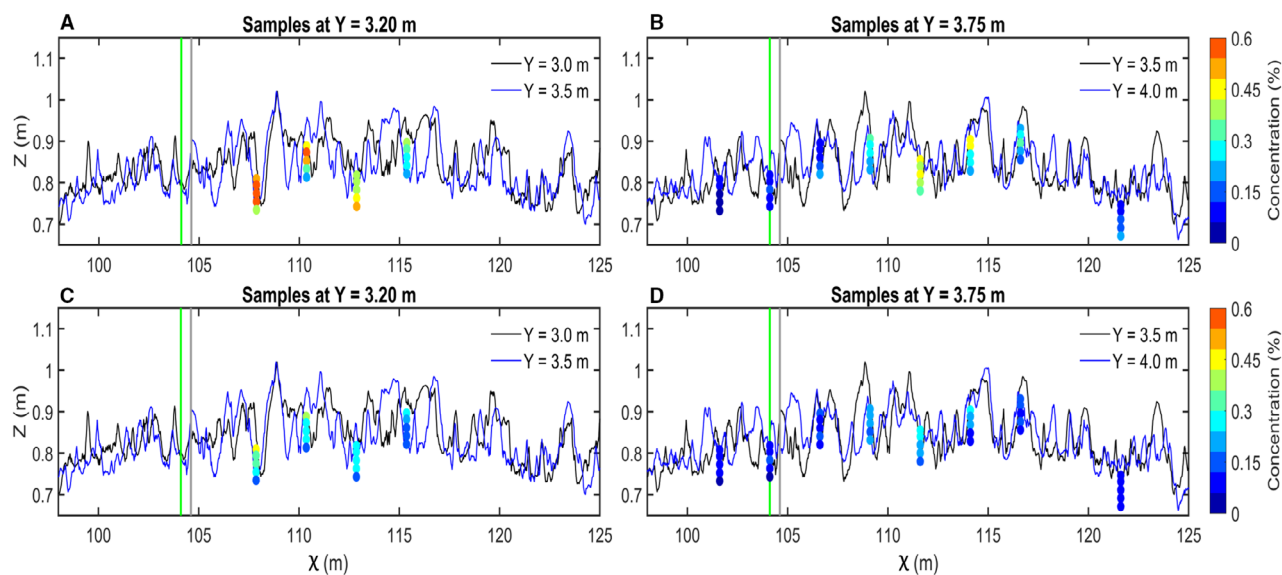


Fig. 8. Vertical distribution of tracer concentrations from samples collected along profiles $Y = 3.20$ m and 3.75 m for the magnetic tracer (A) and (B) and the fluorescent tracer (C) and (D), layers D1 (surface) to D5 (bottom). The solid lines represent the measured bed profiles. The green and grey vertical bars are the initial position of the fluorescent and magnetic tracers, respectively.

Table 2. Tracer centre of mass displacement (CM), average concentration (\bar{C}), recovery rate (R) and net transport rate (Q) for each sampled layer (D1 to D5), and depth-integrated values for magnetic (SIRM, χ) and fluorescent tracers.

Layer	SIRM _{0.6T}			χ			Fluorescent		
	CM _x (m)	\bar{C} (kg/m ³)	R (%)	CM _x (m)	\bar{C} (kg/m ³)	R (%)	CM _x (m)	\bar{C} (kg/m ³)	R (%)
D1 (0–1 cm)	7.55	1.97	4.8	7.85	1.87	4.6	6.59	1.31	9.6
D2 (1–3 cm)	7.48	2.28	11.2	7.54	2.12	10.4	6.56	1.20	17.6
D3 (3–5 cm)	7.16	2.32	11.4	7.32	2.20	10.8	6.21	1.07	15.8
D4 (5–7 cm)	7.35	2.28	11.2	7.40	2.18	10.7	6.10	1.22	17.9
D5 (7–9 cm)	7.30	2.15	10.6	7.55	2.18	10.7	6.50	0.84	12.3
D1–D5	7.37	2.23	49.25	7.52	2.14	47.16	6.39	1.11	73.20
Q ($\times 10^{-5}$ m ² /s)	9.47			9.67			8.22		

between the sand and the tracer allow magnetic tracers to be reliably distinguished and used to track sand transport in natural environments.

Magnetic versus fluorescent tracer particle detection

The scatter plot of tracer concentration normalized by the injected mass of each tracer (Fig. 9), shows that most samples have higher concentrations of fluorescent tracers than magnetic tracers based on SIRM_{0.6T}. The same holds for recovery rates (Table 2), which are much higher for the fluorescent tracer (73%) compared to the magnetic tracers (47% and 49% for the χ and SIRM_{0.6T}, respectively). Beyond uncertainties in the detection approach, the discrepancy in the recovery rates between magnetic and fluorescent particles may be due to two main factors: (i) differences in particle behaviour during the phases of entrainment and transport (magnetic versus fluorescent); and (ii) degree of adherence and resistance to abrasion of the magnetic ink covering the sandy particles. Regarding the first factor, the density of the magnetic particles is slightly higher than that of the fluorescent ones, which could lead to different behaviours of their entrainment and subsequent transport (see *Preparation of tracers* section). However, the vertical distribution pattern of both tracers is similar (Fig. 8), for instance, cores with higher vertical variability of concentration of magnetic tracers (Fig. 8A and B) also have a higher variability of concentration of the fluorescent tracer (Fig. 8C and D). Further, the net transport rates are identical for both magnetic and fluorescent tracers,

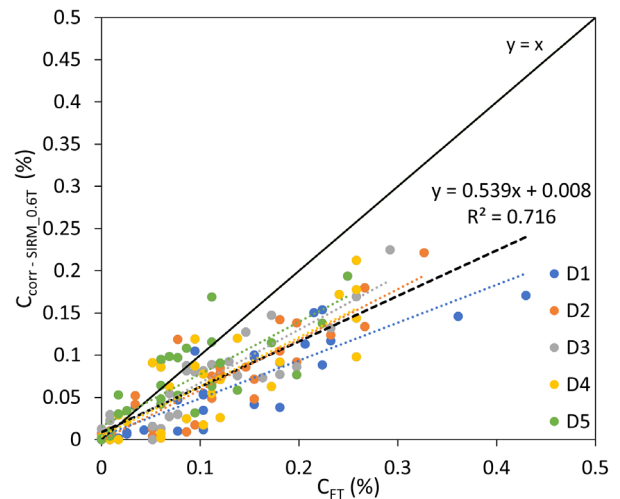


Fig. 9. The relationship between mass normalized magnetic tracer concentration (i.e. concentrations are normalized by the injected mass of each tracer) based on saturation isothermal remanent magnetization (SIRM) ($C_{\text{corr-SIRM}_{0.6T}}$) versus the fluorescent tracer concentration (C_{FT}). The points represent each sample, and each colour corresponds to a different layer. The coloured lines are the respective fit line, and the black dashed line is the fit line of all samples.

also supporting the hypothesis of a similar hydraulic behaviour (Table 2).

Concerning the second factor, Poleykett (2016) showed that the fluorescent ink tracer is robust across a wide range of temporal scales, i.e. the loss of fluorescent ink during transport is minimal. However, the durability of the magnetic coatings used in this study on the sand particles is uncertain. The abrasion of the magnetic tracer during

transport would lead to a reduction in expected values for magnetic susceptibility and magnetization as seen in this study. To evaluate the loss of magnetic coating due to abrasion during transport in the wave flume experiment, an analysis was performed to derive a second IRM calibration curve based on magnetic tracer particles taken from samples after the experiment. The magnetic tracer was separated from the collected bed samples using a Frantz magnetic separator (S.G. Frantz Co., Tullytown, PA, USA). A comparison of SIRM values of the magnetic tracers before and after the experiment shows a difference of 24% (Fig. 10). These

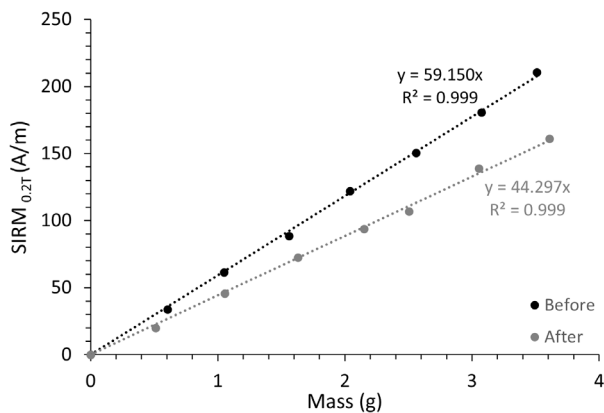


Fig. 10. Calibration curves based on the isothermal remanent magnetization at saturation isothermal remanent magnetization ($SIRM_{0.2T}$) for magnetic tracers in samples before and after the experiment.

results indicate that there was a significant loss of magnetic coating during the experiment.

Uncertainties in tracer particle detection

A number of other possible sources of uncertainty also need to be considered: for example, the density of the sampling grid may not have sufficient resolution to detect extreme values of tracer concentration, the sampling depth may not always be representative of the entire vertical mixing layer, and the presence of an uneven bottom, due to bedforms, might present challenges for the spatial interpolation of data. Some additional issues arose during the experiment (Table 3), and appropriate measures were taken to reduce their impact. For example, during the process of preparation of the magnetic tracer, some aggregates formed, which had to be removed using a sieve. The fluorescent tracer was also previously washed to reduce the surface tension that can affect the results of sediment transport if tracer particles are retained at the water surface. In addition, methodological approaches used in tracer detection could create some differences between the magnetic and fluorescent tracers' results. For example, the range of concentrations used in the calibration has a lower resolution in the fluorescent tracer. The fluorescent tracer detection is also dependent on image acquisition conditions (light and camera resolution), an issue that does not affect the detection of magnetic tracers. The magnetic signal of the natural quartz sand used in the experiment is very

Table 3. Aspects to take into account during the preparation and detection of magnetic and fluorescent tracers: Symbology: + – very low impact; ++ – low impact; NA – not applicable; Unk – unknown.

Aspects	Magnetic tracer		Fluorescent tracer	
		Preventative measures		Preventative measures
Preparation				
Aggregates formation	++	Tracer was sieved	+	–
Tracer density	++	–	+	–
Dry sand floatability (surface tension)	+	Tracer was washed	++	Tracer was washed
Tracer detection				
Separation of grain-size fractions	NA	–	Unk	Probably low
Range of concentrations used in calibration	+	–	++	–
Image acquisition conditions (light and camera resolution)	NA	–	++	–
Magnetic signal of native sand	+	Artificial quartz sand used	NA	–

weak and is thus unlikely to affect the magnetic tracer results.

Particle transport rate prediction using different tracer techniques

Concentrations, normalized to account for the difference in tracer recovery rates, were shown to be independent of the measured property (χ , $SIRM_{0.6T}$ and FT) with similar spatial concentration patterns (Fig. 11). The results obtained with the three approaches are comparable, showing good agreement (within 16%) in estimates for the centre of mass displacement and net transport rates (Table 2). The net transport occurred in the

direction of wave propagation due to non-linear and streaming effects (Ferreira *et al.*, 2023).

Comparison of the implementation of different tracer techniques

The results allow for assessment of the advantages and disadvantages of the magnetic tracer method. This assessment was achieved by the analysis of the magnetic tracer results and comparisons with results using a standard approach utilizing fluorescent tracers. Results obtained using either magnetic or fluorescent tracers are equivalent (see Fig. 11), although there were some differences in recovery rates, as was

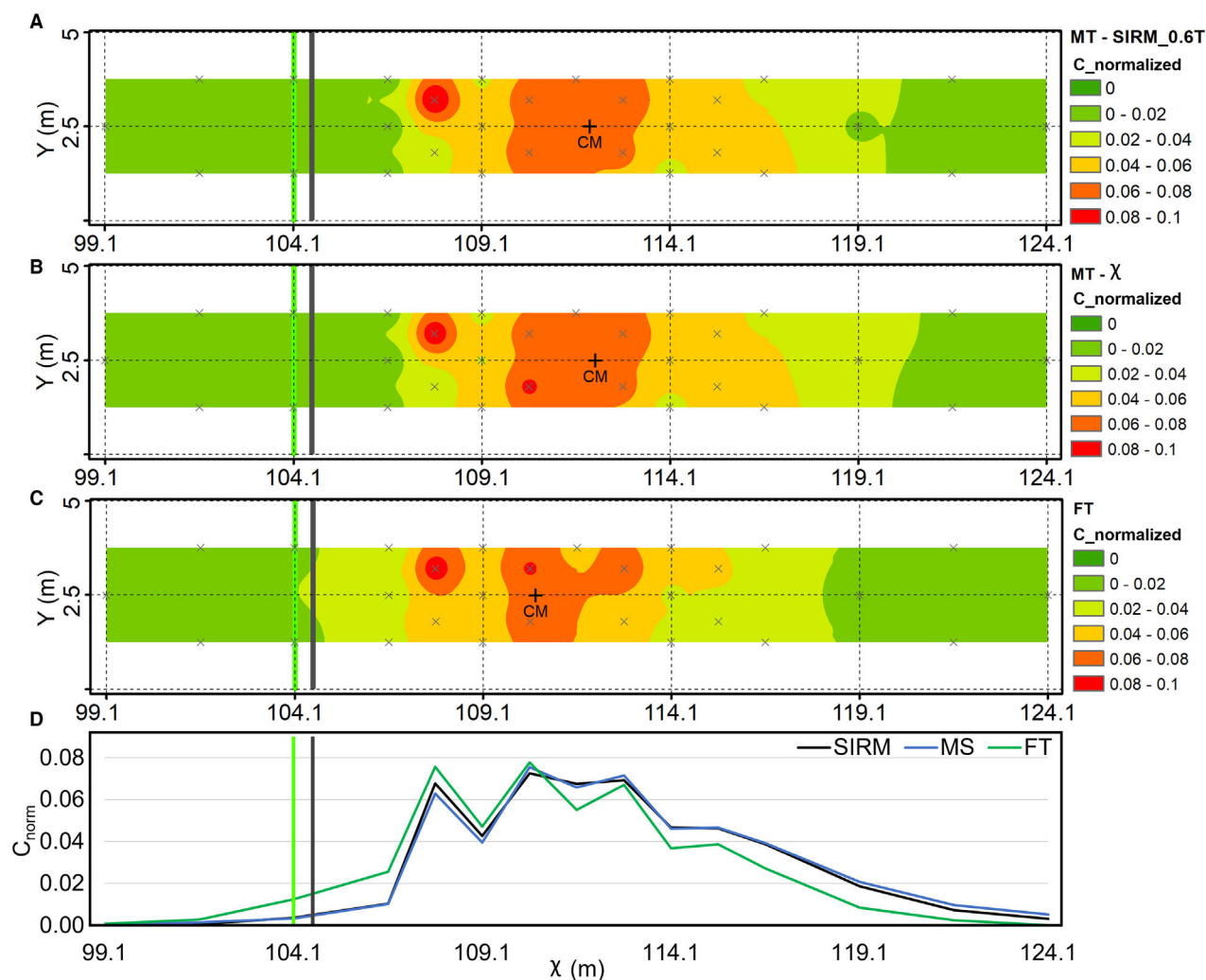


Fig. 11. Horizontal distribution patterns for tracer normalized concentrations based on: (A) magnetic tracer measured by isothermal remanent magnetization ($SIRM_{0.6T}$); (B) magnetic tracer measured by magnetic susceptibility (χ); (C) fluorescent tracer technique (FT); and (D) across-stream averaged concentration based on each approach. Concentrations are normalized with respect to the total tracer concentration. Black crosses indicate sample locations and the green and grey lines the location of fluorescent and magnetic tracer injection lines, respectively.

justified by the detection of some abrasion of the magnetic ink coating (see explanation above). Also, the fluorescent tracer method is based on single particle detection (allowing the determination of grain size) while the detection of the magnetic tracer concentration is integrated in the volume of a sample.

The cost, effort and time for the implementation of the magnetic tracer in the experiment was similar to that for fluorescent tracers. The magnetic tracers only required some additional time for the drying of the magnetic pigment and for sieving of aggregates formed during the coating process (6 h, depending on weather conditions). Notwithstanding, the most appealing feature of the magnetic tracer method is the ease of detection and sample processing in the laboratory, which required less than 10 min per sample compared to 15 min per sample for fluorescent tracers. The study provides support that magnetic tracers have the potential to be easily applied in the field (Galloway *et al.*, 2012; Poleykett *et al.*, 2018; Pearson *et al.*, 2021). The use of tracers constitutes a promising technique to assess sediment transport. Furthermore, the results and data acquired in this experiment provide a dataset that may be used to calibrate empirical and numerical models.

CONCLUSIONS

This study provides the first detailed comparison between the use of magnetic and fluorescent tracers in a controlled laboratory environment to estimate net transport rates. The two techniques yield consistent results, particularly in estimating sediment transport under full-scale wave conditions in a flume experiment (trochoidal waves with 1.5 m wave height and 7 s period). Notably, the mass-dependent magnetic properties like magnetic susceptibility and saturation isothermal remanence emerge as reliable indicators of the relative abundance of the transported magnetic tracers in the bulk samples. The comparison of the results with those obtained using fluorescent tracers show a systematic difference of about 24% in terms of recovery rates, which may be explained by the loss of magnetic coating during transport. Exploring alternative magnetic pigments may reduce the problem of coating loss during sediment transport. Despite the recovery rates discrepancy, findings suggest that both magnetic and fluorescent tracers display a similar transport behaviour, as indicated by overall similarities in vertical and horizontal distribution patterns. Net transport rates derived

from both tracer types were also in broad agreement (<16% difference), indicating transport in the direction of wave propagation. The study confirms that the use of magnetic tracers represents a time-effective and potentially valuable method for studying sediment transport in both laboratory and natural environments. The results provide a dataset that may be used for calibrating empirical and numerical models.

ACKNOWLEDGEMENTS

Funding was provided by CESAM (UIDP/50017/2020 + UIDB/50017/2020 + LA/P/0094/2020), IDL [UIDB/50019/2020 (<https://doi.org/10.54499/UIDB/50019/2020>) + UIDP/50019/2020 (<https://doi.org/10.54499/UIDP/50019/2020>) + LA/P/0068/2020 (<https://doi.org/10.54499/LA/P/0068/2020>)], by FCT/MCTES through national funds (PIDDAC), and FEDER within the PT2020 Partnership Agreement and Compete 2020. Work performed under the scope of SANDTRACK project (POCI-01-0145-FEDER-031779) funded by FEDER, through COMPETE2020 – Programa Operacional Competitividade e Internacionalização (POCI), and by national funds (OE), through FCT/MCTES. The flume experiments were funded through the project STENCIL – Strategies and Tools for Environment-friendly Shore Nourishment as Climate Change Impact Low-Regret Measures (German Federal Ministry of Education and Research/BMBF, contract no. 03F0761). Thanks are due to Stefan Schimmels for all the support during the experiments and for providing the bed level measurements data. All the participants in the GWK experiments are gratefully acknowledged. S. R. is financed by FCT (SFRH/BD/129079/2017). Thanks are due to the journal reviewers (Stuart Pearson and Paul Myrow) and the editors for their constructive comments and thoughtful revision.

DATA AVAILABILITY STATEMENT

The data that supports the findings of this study are available in the [Supplementary Material](#) of this article.

REFERENCES

- Abecasis, F., Matias, M.F., Reis De Carvalho, J.J. and Vera-Cruz, D. (1962) Methods of determining sand and silt movement along the coast, in *Estuaries and in Maritime*

- Rivers, *Technical Paper*, pp. 186. Laboratório Nacional de Engenharia Civil (LNEC): Lisboa.
- Black, K.S.** (2012) Using sediment tracers to map sediment transport pathways. *Partrac*, **44**, 1–18.
- Black, K.S., Athey, S., Wilson, P. and Evans, D.** (2007) The use of particle tracking in sediment transport studies: a review. *J. Geol. Soc. Lond.*, **274**, 73–91.
- Blott, S.J. and Pye, K.** (2001) Gradstat: a grain size distribution and statistics package for the analysis of unconsolidated sediments. *Earth Surf. Process. Landf.*, **26**, 1237–1248.
- Boscia, D.** (2021) *Dynamics and Transport of Sand Mixtures in Oscillatory Flows*. PhD Thesis, University of Aberdeen.
- Bosnic, I., Cascalho, J., Taborda, R., Drago, T., Hermínio, J., Rosa, M., Dias, J. and Gareil, E.** (2017) Nearshore sediment transport: coupling sand tracer dynamics with oceanographic forcing. *Mar. Geol.*, **385**, 293–303.
- Christensen, E.R. and Bhunia, P.K.** (1986) Modeling radiotracers in sediments: comparison with observations in Lakes Huron and Michigan. *J. Geophys. Res.*, **91**(C7), 8559–8571.
- Ciavola, P. and Grotoli, E.** (2019) Tracers and coarse sediment. In: *Encyclopaedia of Coastal Science. Encyclopaedia of Earth Sciences Series* (Eds Finkl, C.W. and Makowski, C.). Springer, Cham. https://doi.org/10.1007/978-3-319-93806-6_330.
- Crickmore, M.J.** (1976) Tracer techniques for sediment studies; their use, interpretation and limitations. In: *Diamond Jubilee Symposium on Modelling Techniques in Hydraulic Eng.*, Vol. 1, Paper A13. Central Power and Water Research, Pune.
- Dearing, J.A.** (1999) *Environmental Magnetic Susceptibility Using the Bartington MS2 System*.
- Drapeau, G. and Long, B.** (1985) Measurements of bedload transport in the nearshore zone using radioisotopic sand tracers. *Proceedings of the Coastal Engineering Conference*, **2**, 1252–1264 <https://doi.org/10.1061/9780872624382.086>.
- Egli, R.** (2004) Characterization of individual rock magnetic components by analysis of remanence curves, 1. Unmixing natural sediments. *Stud. Geophys. Geod.*, **48**, 391–446.
- Ferreira, C.C.** (2022) Sediment Transport in Coastal Environments with Mixed Sand Beds. PhD thesis. University of Aveiro. <http://hdl.handle.net/10773/33640>.
- Ferreira, C.C., Silva, P.A., Bernabeu, A.M. and Abreu, T.** (2023) Transport of heterometric sediments in wave-dominated flows – Tracer experiments. *Mar. Geol.*, **459**, 107042.
- Folk, R.L.** (1966) A review of grain-size parameters. In: *Sedimentology*, Vol. 6, pp. 73–93. John Wiley & Sons, Ltd, London.
- Galloway, E., Trenhaile, A.S., Cioppa, M.T. and Hatfield, R.G.** (2012) Magnetic mineral transport and sorting in the swash-zone: Northern Lake Erie, Canada. *Sedimentology*, **59**, 1718–1734.
- Garzanti, E. and Andò, S.** (2019) Heavy minerals for Junior Woodchucks. *Minerals*, **9**, 148.
- Ingle, J.C.** (1966) The movement of beach sand: An analysis using fluorescent grains. In: *Developments in Sedimentology*, Vol. 5, pp. III–VIII. Elsevier Pub.: Colorado.
- Inman, D.L. and Chamberlain, T.K.** (1959) Tracing beach sand movement with irradiated quartz. *J. Geophys. Res.*, **64**, 41–47.
- Kruiver, P.P., Dekkers, M.J. and Heslop, D.** (2001) Quantification of magnetic coercivity components by the analysis of acquisition curves of isothermal remanent magnetisation. *Earth Planet. Sci. Lett.*, **189**, 269–276.
- Maxbauer, D.P., Feinberg, J.M. and Fox, D.L.** (2016) MAX UnMix: A web application for unmixing magnetic coercivity distributions. *Comput. Geosci.*, **95**, 140–145.
- Miller, M.C. and Komar, P.D.** (1979) Measurements of sand spreading rates under near-bottom wave orbital motions. *J. Geol.*, **87**, 593–608.
- Mu, L.** (2009) Thiessen polygon. In: *International Encyclopedia of Human Geography*, pp. 231–236. Elsevier, Amsterdam.
- O'Donoghue, T., Doucette, J.S., van der Werf, J.J. and Ribberink, J.S.** (2006) The dimensions of sand ripples in full-scale oscillatory flows. *Coast. Eng.*, **53**, 997–1012.
- Oldfield, F., Thompson, R. and Dickson, D.P.E.** (1981) Artificial magnetic enhancement of stream bedload: a hydrological application of superparamagnetism. *Phys. Earth Planet. Inter.*, **26**, 107–124.
- Pantin, H.M.** (1961) Magnetic concrete as an artificial tracer mineral. *NZ J. Geol. Geophys.*, **4**, 424–433.
- Pearson, S.G., van Prooijen, B.C., Poleykett, J., Wright, M., Black, K. and Wang, Z.B.** (2021) Tracking fluorescent and ferrimagnetic sediment tracers on an energetic ebb-tidal delta to monitor grain size-selective dispersal. *Ocean Coast. Manag.*, **212**, 105835.
- Poleykett, J.** (2016) The Development of Dual Signature, Fluorescent- Magnetic Sediment Tracing Technology. PhD Thesis. Lancaster University.
- Poleykett, K., Friend, P.L., Black, K.S., Wright, M.R., Davidson, M.A. and Morton, P.** (2018) The application of an active sediment tracing technique to assess the efficacy of nearshore placement of dredged material for beach nourishment purposes. *Proceedings of the Western Dredging Association Dredging Summit & Expo '18*, 1(June), 15.
- van der Post, K.D., Oldfield, F. and Voulgaris, G.** (1995) Magnetic tracing of beach sand: preliminary results. *Proceedings of International Conference Coastal Dynamics '94*, 323–334.
- Schretlen, J.L.M.** (2012) Sand Transport under Full-Scale Progressive Surface Waves. 2012. PhD Thesis. University of Twente <https://doi.org/10.3990/1.9789462030619>.
- Silva, A., Taborda, R., Rodrigues, A., Duarte, J. and Cascalho, J.** (2007) Longshore drift estimation using fluorescent tracers: New insights from an experiment at Comporta Beach, Portugal. *Mar. Geol.*, **240**, 137–150.
- Soulsby, R.L. and Damgaard, J.S.** (2005) Bedload sediment transport in coastal waters. *Coast. Eng.*, **52**, 673–689.
- Ventura, E., Nearing, M.A. and Norton, L.D.** (2001) Developing a magnetic tracer to study soil erosion. *Catena*, **43**, 277–291.
- Vila-Concejo, A., Ferreira, Ó., Ciavola, P., Matias, A. and Dias, J.M.A.** (2004) Tracer studies on the updrift margin of a complex inlet system. *Mar. Geol.*, **208**, 43–72.
- van der Werf, J.J., Staudt, F., Posanski, D., van de Wardt, W., van der Zanden, J., Vermeulen, B., Ribberink, J.S. and Schimmels, S.** (2019) Understanding and modelling wave-driven mixed sand transport. *Coast. Sed.*, **2019**, 788–801.
- White, T.E.** (1998) Status of measurement techniques for coastal sediment transport. *Coast. Eng.*, **35**, 17–45.
- Wilson, G.W.** (2018) Anomalous diffusion of sand tracer particles under waves. *J. Geophys. Res. Earth*, **123**, 3055–3068.
- Yasso, W.E.** (1966) Formulation and use of fluorescent tracer coatings in sediment transport studies. *Sedimentology*, **6**, 287–301.

Manuscript received 23 December 2022; revision accepted 4 January 2024

Supporting Information

Additional information may be found in the online version of this article:

Appendix S1. Table of measurement values of SIRM and χ for samples with a known mass of magnetic tracers used to establish calibration curves.

Appendix S2. Table of data used in the study including sample locations, SIRM measurement values, χ values and the respective concentrations.